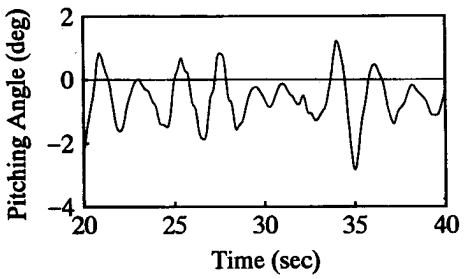

Fig. 12. Estimate of pitching angle.

The computational time of the proposed measurement system was about 30 ms with TOSHIBA EWS (engineering work station) AS4080 from the acquisition of the sensor outputs to the measurement of the ship's attitude. If advanced computer technology will be used or the sampling time is a little enlarged, a microcomputer will be available for the on-line measurement. Furthermore, by increasing the number of the candidates, the accuracy of the measurement is much more improved, and for that aim a multiprocessor technique which enables the parallel computation in a bank of Kalman filters is efficiently used.

V. Conclusion

The paper proposed an on-line automatic measurement system which accurately measured the heaving, rolling, and pitching of ship by adequately processing the outputs of four accelerometers and one inclinometer appropriately located on the ship. By modeling the heaving, rolling, and pitching signals by adequate linear dynamic systems and using a bank of Kalman filters, on-line accurate measurement of ship's attitude was realized. Further improvement of the accuracy of the measurement is achieved by increasing the number of the candidates used in a bank of Kalman filters.

References

[1] S. Tanaka, "On automatic attitude measurement system for ships using servo-type accelerometers (in Japanese)," *Trans. SICE*, vol. 27, pp. 861–869, Aug. 1991.

[2] H. Akaike, "Power spectrum estimation through autoregressive model fitting," *Annu. Inst. Stat. Math.*, vol. 21, pp. 407–419, 1969.

[3] S. Minami, Ed., *Processing of Waveforms for Scientific Measurement* (in Japanese). Tokyo: CQ Press, 1986, sec. 9, pp. 166–180.

[4] Y. Takahashi, M. J. Rabins, and D. M. Auslander, *Control and Dynamic Systems*. Reading, MA: Addison-Wesley, 1971.

[5] R. E. Kalman, "A new approach to linear filtering and prediction problems," *Trans. ASME, J. Basic Eng.*, vol. 82, pp. 35–45, Mar. 1960.

[6] S. Arimoto, *Kalman Filter* (in Japanese). Tokyo: Sangyo Tosho, 1977, sec. 3, pp. 53–88.

Isolation of Resonance in Acoustic Backscatter from Elastic Targets Using Adaptive Estimation Schemes

Mahmood R. Azimi-Sadjadi, JoEllen Wilbur, and Gerald J. Dobeck

***Abstract*— The problem of underwater target detection and classification from acoustic backscatter is the central focus of this paper. It has been shown that at certain frequencies the acoustic backscatter from elastic targets exhibits certain resonance behavior which closely relates to the physical properties of the target such as dimension, thickness, and composition. Several techniques in both the time domain and frequency domain have been developed to characterize the resonance phenomena in acoustic backscatter from spherical or cylindrical thin shells. The purpose of this paper is to develop an automated approach for identifying the presence of resonance in the acoustic backscatter from an unknown target by isolating the resonance part from the specular contribution. An adaptive transversal filter structure is used to estimate the specular part of the backscatter and consequently the error signal would provide an estimate of the resonance part. An important aspect of this scheme lies in the fact that it does not require an underlying model for the elastic return. The adaptation rule is based upon fast Recursive Least Squares (RLS) learning. The approach taken in this paper is general in the sense that it can be applied to targets of unknown geometry and thickness and, further, does not require any *a priori* information about the target and/or the environment. Test results on acoustic data are presented which indicate the effectiveness of the proposed approach.**

I. Introduction

The theory of acoustic resonance scattering from submerged elastic shells has received considerable attention [1]–[13]. In the acoustic scattering response, the mid-frequency band is of particular interest in the characterization of small elastic targets [1]–[4]. This band is dominated by the specular reflection and the lowest order symmetric and anti-symmetric Lamb modes which propagate on the shell. The resonant backscatter attributed to these modes have been found to offer viable signature clues for identifying submerged elastic targets [3], [4]. However, identification of the elastic response associated with the mid-frequency region is nontrivial, especially for targets of arbitrary geometry. That is, the resonant return can be difficult to isolate from the specular component and is often buried in the noise. When the target parameters are not known *a priori* a large time-bandwidth product (TB) may be sent to sufficiently excite the resonant modes. However, the specular and resonant responses in the acoustic backscatter may overlap both temporally and spectrally. This, coupled with other factors in a real target detection environment, such as sensitivity of the sensors to the environmental and operating conditions, nonrepeatability of the target signatures, competing clutter objects having similar response as the actual targets, and lack of *a priori* information about the actual targets, create a complex signal processing problem.

Various schemes have been proposed [7]–[13] to extract resonance information from the acoustic backscatter from a thin spherical shell submerged in water. These either use temporal information or transform domain processing to determine the presence of resonances.

Manuscript received November 13, 1993; revised November 28, 1994. The work of M. R. Azimi-Sadjadi was supported by the ASEE-ONR program under the High Area Rate Recon. Project. The work of J. Wilbur and G. J. Dobeck was supported by the ONR.

M. R. Azimi-Sadjadi is with the Department of Electrical Engineering, Colorado State University, Fort Collins, CO 80523 USA.

J. Wilbur and G. J. Dobeck are with the Research and Technology Department, Coastal Systems Station, Panama City, FL 42307-5000 USA.

IEEE Log Number 9414015.

Murphy *et al.* [7] separated the resonant part from the "background" given the impulse response of a fluid-loaded elastic spherical shell by formulating the background amplitude as that of a rigid body. This method is shown to be particularly effective for thick spherical shells. In the work by Ripoche *et al.* [8] a large aspect ratio aluminum cylindrical shell is insonified by an incident burst of several cycles. The frequency of the incident is then varied slowly and the spectrum of the acoustic backscatter is examined. The position of the resonances and their associated "mode number" are confirmed experimentally by studying the corrected and gated spectrum of the backscattered data. De-Billy [9] used short pulses and a similar approach to determine the resonance of submerged elastic cylindrical wires. A joint time-frequency examination of the impulse response of a thin spherical shell is investigated in [11] using the Wigner-Ville distribution. This time-frequency representation provides localization of the signal energy along both the time and frequency axis. In [12] Wilbur and Kargl applied a wavelet transform to detect the resonance corresponding to the mid-frequency enhancement of a thin spherical shell submerged in water and surrounded by biologics. It is shown, in the simulation results in [12], that the mid-frequency enhancement corresponding to the lowest order symmetric Lamb mode can be identified through the wavelet decomposition in the acoustic return from a thin spherical shell surrounded by biologics. More specifically, the specular reflection manifests itself in the form of a persistent ridge along all dilations while the acoustic backscatter corresponding to the subsonic branch of the lowest order anti-symmetric Lamb wave or the mid-frequency enhancement region yields a rather localized ridge in the wavelet plane. The position of the ridge moves to lower frequencies as the shell thickness increases.

The purpose of this paper is to present an automated approach for isolating the resonant response from the acoustic backscatter of a submerged elastic target of unknown shape. The approach uses an adaptive filtering process which allows for resonance extraction directly from backscattered data. Although resonance extraction has been studied and developed extensively for spherical shells, large aspect ratio cylindrical shells and cylinders with spherical end caps, the problem is difficult when applied to an elastic target of arbitrary geometry for which the poles of the resonances are not known *a priori*. This is especially true when the specular and resonant returns overlap in both the time and frequency domains. The method in this paper is general in the sense that it does not require generation of the impulse response or the transfer function and can be applied to a target of unknown geometry and thickness. The only assumptions made by the approach are: the specular is more correlated to the incident than is the resonance, and while the specular and resonance may overlap in time, the onset of the specular proceeds that of the resonance. An adaptive transversal filter structure is used to estimate the specular part of the backscatter and extract the hidden resonance characteristics of the elastic objects. The estimate of the specular part is provided at the output of the system and consequently the error signal extracts the resonant part. The adaptation rule is based upon the Recursive Least Squares (RLS) learning which does not have the accuracy-speed trade-off associated with the standard Least Mean squares (LMS) algorithm. The adaptive processor is first tested on acoustic backscatter data collected from a submerged spherical shell. It is then applied to acoustic backscatter from a submerged elastic target whose shape is that of a tapered, notched cylinder with flattened ends and rivets. The results are then compared to those collected for a nontarget concrete chunk of a size similar to that of the target. Using this scheme detection and classification can be facilitated by applying various feature extraction schemes to the isolated resonant part. The extracted information may then be applied to a classifier to perform the classification task [13], [14].

II. Acoustic Resonance Characterization

The problem of acoustic scattering from submerged elastic targets and in particular spherical and cylindrical shells has attracted considerable interest [1]–[13] in the last decade. It has been shown that at certain frequencies the acoustic backscatter from an elastic target exhibits certain resonance behavior which closely relates to the physical properties of the target such as dimension, thickness, and composition. Although the theoretical and experimental results for a wide frequency range have concentrated on thin spherical shells, thorough understanding of these results would certainly help in dealing with subtleties associated with targets of more complicated shapes. In what follows the phenomenon of resonance in acoustic backscattering from a spherical thin shell will be briefly reviewed in order to establish a basis for understanding of this important property of elastic objects. A more thorough discussion can be found in [1].

The far-field steady-state backscattered pressure of an evacuated elastic spherical shell immersed in water can be written [2] as

$$p(t) = (a/2R)\,\mathrm{Re}\left\{I_{\mathrm{inc}} e^{jk(R-ct)} f(ka)\right\} \tag{1}$$

where $ka = 2\pi a/\lambda$; k represents the wave number, λ the wavelength of the incident wave; a is the outer radius of the shell; R is the radial distance from the shell; c is the phase velocity; I_{inc} is the amplitude of the incident planar wave and $f(ka)$ is the "backscattering form function" of the shell which is given by

$$f(ka) = \frac{2}{jka}\sum_{n=0}^{\infty}(-1)^n(2n+1)\frac{B_n(ka)}{D_n(ka)} \tag{2}$$

where $B_n(ka)$ and $D_n(ka)$ are 5×5 determinants whose elements are linear combinations of spherical Bessel and Hankel functions of the first kind [6]. These elements contain all the material parameter dependence of $f(ka)$ and they also depend on the shell's radius and thickness. Define the dimensionless time T as

$$T = (ct - R)/a. \tag{3}$$

An increment in T of one unit corresponds to the amount of time it takes for sound to travel a distance equal to the shell radius a in the surrounding water. Now, (1) can be rewritten as

$$p(T) = (a/2R)\,\mathrm{Re}\left\{I_{\mathrm{inc}} e^{-jxT} f(x)\right\} \tag{4}$$

where $x := ka$ is the dimensionless frequency. As can be seen in this case the transient scattering is determined by shifting the form function in phase. However, for more general cases of the incident wave such as sinusoidal or FM modulated bursts the scattered signal can be written using Fourier analysis as [2]

$$p(T) = (a/2R)\,\mathrm{Re}\left\{\frac{1}{\pi}\int_0^{\infty} I(x) f(x) e^{-jxT}\,dx\right\} \tag{5}$$

where $I(x)$ represents the spectrum of the incident wave. The Fourier integral in (5) can be performed using the Discrete Fourier transform (DFT) via fast Fourier transform (FFT) algorithms [2].

Fig. 1(a) shows the transfer function for a steel spherical shell where the ratio of the shell thickness to outer radius is 2%. The contribution corresponding to the specular reflection yields a broadband nearly flat spectral response over the passband of the transmit pulse. In the low frequency region ($0 < ka \leq 10$) where the acoustic wavelength is comparable to the shell diameter, the nature of the coupled-fluid elastic waves depends strongly on the shell geometry and thickness. For "very thin" shells ($h < 0.005\ a$) there is evidence [3] of only one elastic mode and the transfer function exhibits a relatively broad resonance peak associated with the breathing mode and two dips; while for "thin" shells ($0.01\ a \leq h \leq 0.1\ a$) there are generally two elastic modes and the transfer function is characterized

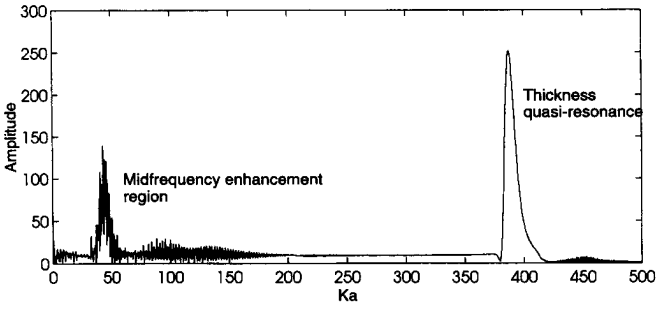

(a)

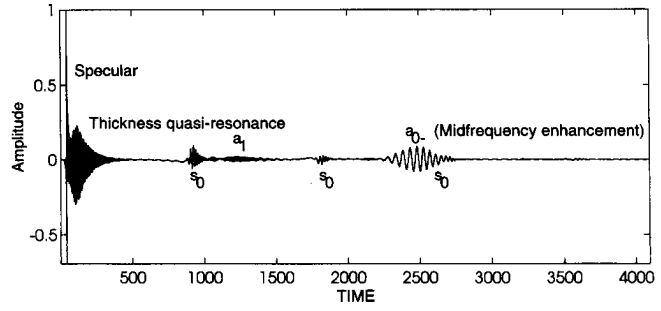

(b)

Fig. 1. (a) Transfer function of 2% spherical shell. (b) Impulse response of 2% spherical shell.

by a large number of strong, high-Q resonance peaks, and a smaller number of broad dips. For "thick" shells ($0.2\ a < h$), however, the pronounced high-Q resonance is no longer evident as the breathing mode becomes damped [3]. The mid-frequency region in which the acoustic wavelength is small compared to the shell radius but large compared to the shell thickness is dominated by the s_0 and a_0 modes. The lowest order symmetric Lamb mode, designated s_0, yields high-Q resonances of regular spacing which is inversely related to shell diameter. The symmetric Lamb wave contributions maintain a bi-phase relationship with the specular return which manifests itself in the transfer function in the form of narrow-band notches or nulls. The lowest order anti-symmetric Lamb wave, designated a_0, bifurcates into two distinct modes around the shell: the subsonic, a_{0-}, and the supersonic, a_{0+}, Lamb modes. The subsonic branch of the anti-symmetric Lamb mode, a_{0-}, is characterized in the target transfer function by narrow-band tones atop a broad nearly Gaussian envelope. The center frequency of the Gaussian is inversely related to shell diameter and thickness. The elastic resonance associated with the a_{0-} portion is referred to as the mid-frequency enhancement. For thick shells, this enhancement, if it exists, moves to lower frequency regions in the shell transfer function. The mid-frequency enhancement is the consequence of the constructive interference among the a_{0-} resonances. In the high frequency region where the wavelength is of the order of the shell thickness, there are generally a large number of elastic modes. In particular, the s_1 symmetric Lamb wave is associated with a second prominent peak known as the thickness quasi-resonance.

In [3] a method is developed using the residue theorem to analyze the scattering behavior through the study of the pole locations of the scattering amplitude. It was observed that the poles associated with s_0 lie close to the real axis. This mode is bi-phase to the specular component resulting in notches at regular spacings of $4ka$ in the transfer function in Fig. 1(a). The regular spacing between these dips corresponds to circumnavigations around the shell. That is, the s_0 mode contribution to the impulse response function is a decaying

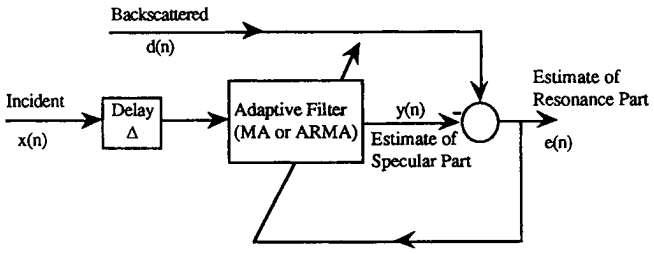

Fig. 2. Adaptive structure for estimation of resonance part.

sequence of pulses whose spacing relates directly to shell diameter. As shell thickness decreases the effects will be less evident. At high er frequencies the poles move closer to the real axis and this mode becomes more visible again. For the subsonic portion of the lowest order anti-symmetric Lamb mode, a_{0-}, the poles associated with the high-Q and nonoverlapping resonances are close to the real axis and tend to have a strong effect on the scattering. However, as frequency increases beyond a certain threshold which depends on the thickness of the shell, the poles move rapidly into the complex plane (with increasing frequency and order), and become broader and tend to have significant overlap with other poles of the scattering amplitude. The poles associated with the supersonic portion of the lowest order anti-symmetric Lamb mode, a_{0+}, are found to be sufficiently deep in the complex plane so that they do not have a strong influence on the scattering amplitude.

Fig. 1(b) shows the corresponding impulse response for the 2% steel shell. This impulse response exhibits several prominent parts which are associated with different scattering phenomena [2]–[6]. The leading spike is associated with the specular reflection (direct geometrically reflected return) on the outer surface of the shell. This is followed by a decaying sequence which is partly attributed to the first order symmetric Lamb wave (s_1) and partly due to the transmitted bulk waves undergoing multiple reflections between shell surfaces. This contribution is in the high frequency region and is sometimes referred to as the "thickness quasi-resonance" [4]. The echos labeled by s_0 and a_1 are associated with the lowest symmetric Lamb wave and the first order supersonic anti-symmetric Lamb wave, respectively. The mid-frequency enhancement corresponds to those prominent oscillations designated by a_{0-}.

In the next section a new approach for identifying the presence of resonance in the acoustic backscatter from a target of unknown geometry is introduced. This method uses an adaptive filter structure to isolate the resonance part from the specular contribution.

III. Adaptive Signal Detection and Parameter Estimation

Using the conventional detection and estimation techniques generally requires some *a priori* information on the signal and noise/clutter. Often, this information is not available in a real-life environment. In such environments, the application of adaptive signal processing schemes [14] becomes very attractive. The adaptive detector and estimator should be designed in such a way that the changes in the statistical characteristics of the signal and noise can be taken into account in the structure of the adaptive system. In this manner the system is capable of adjusting itself to a new environment and consequently providing more robust target detection and classification.

The structure of the adaptive system used for separating the hidden resonance in the acoustic backscatter is shown in Fig. 2. The reference input to the adaptive system is the incident waveform while the desired signal is the backscattered. In this way, the adaptive system produces an output which is the estimate of the specular part and the

error signal would provide an estimate of the resonance part. There are two principal ideas behind the development of this structure: 1) the specular part of the acoustic backscatter is more correlated with the incident than the resonance (elastic) part, and 2) there is always a time delay between the onset of the specular part and that of the resonance part. Thus, provided that the learning is fast enough, during this period of time the adaptive system produces an output which is an accurate estimate of the specular part. Since the system has infinite memory and further the specular part is more correlated with the input (incident) the system continues to provide a good estimate of the specular part even after the resonance has appeared. As a result, the error signal provides an estimate of the resonance part of the backscattered. Note that the delay Δ is provided to account for the actual delay between the incident and the backscattered. For spherical shells this time delay can be evaluated [2] theoretically from the knowledge of the speed of sound in the water and the group velocity associated with the carrier frequency of the tone burst.

If the adaptive system is of moving average (MA) type [14] with tap weights denoted by $w_i(n)'s$ for $\forall i \in [0, N-1]$, and $n \in [0, P-1]$ where N and P, respectively, represent the filter order and the number of points in the signal, then the output of the filter at time n is the weighted sum of the N present and past input samples $x(k)'s$, $k \in [n, n-N+1]$, weighted by the associated tap weight, $w_k(n-1)$. In vector form the expression for the output $y(n)$ is given by

$$y(n) = \boldsymbol{W}^t(n-1)\boldsymbol{X}(n) \tag{8}$$

where $\boldsymbol{X}(n)$ and $\boldsymbol{W}(n-1)$ represent the input and weight vectors, respectively, i.e.,

$$\boldsymbol{W}(n-1) = [w_0(n-1)w_1(n-1)\cdots w_{N-1}(n-1)]^t \tag{9a}$$

$$\boldsymbol{X}(n) = [x(n)x(n-1)\cdots x(n-N+1)]^t. \tag{9b}$$

As can be observed from (8), the output at time n, i.e., $y(n)$ is estimated using the weights at time $(n-1)$. Now, using the current sample of the desired signal, $d(n)$, the weights can be updated using a weight adaptation rule for transversal filter structures [14]. Owing to the inherent benefits of the RLS adaptation rule which include speed of convergence, accuracy in estimation, variable and data dependent step size, robustness in presence of noise and independency of the performance on data covariance matrix, we have used this learning scheme throughout this paper. In addition, the simplicity of the architecture of the RLS learning together with the above-mentioned benefits makes this algorithm ideal for real-life implementation.

The weight updating equations using the RLS scheme are given in order as [14]:

$$\boldsymbol{K}(n) = \frac{\boldsymbol{P}(n-1)\boldsymbol{X}(n)}{\mu + \boldsymbol{X}^t(n)\boldsymbol{P}(n-1)\boldsymbol{X}(n)} \tag{10a}$$

$$e(n) = d(n) - y(n) = d(n) - \hat{\boldsymbol{W}}^t(n-1)\boldsymbol{X}(n) \tag{10b}$$

$$\hat{\boldsymbol{W}}(n) = \hat{\boldsymbol{W}}(n-1) + \boldsymbol{K}(n)e(n) \tag{10c}$$

$$\boldsymbol{P}(n) = \mu^{-1}[I - \boldsymbol{K}(n)\boldsymbol{X}^t(n)]\boldsymbol{P}(n-1) \tag{10d}$$

where $\hat{\boldsymbol{W}}$ is the estimate of the weight vector $\boldsymbol{W}$; $e(n)$ is the estimation error (resonant part); $\boldsymbol{K}(n)$ is the gain vector; $\boldsymbol{P}(n)$ is the inverse of the input data covariance matrix and μ is the "forgetting factor" which determines the memory $(M = 1/(1-\mu))$ of the adaptation process and $0 < \mu \leq 1$. Generally, for stationary processes μ is chosen to be unity (i.e., infinite memory) which corresponds to standard LS solution, while for nonstationary processes where limited memory is more desirable $0.95 \leq \mu \leq 0.99$. Note that in our application we require infinite memory in order to provide a consistent estimate of the specular component even though the backscattered is a nonstationary process. The process starts with a set of initial values for $\boldsymbol{P}(0)$ and $\hat{\boldsymbol{W}}(0)$. In this paper, we have chosen $\boldsymbol{P}(0) = \delta^{-1}\boldsymbol{I}$ and $\hat{\boldsymbol{W}}(0) = \boldsymbol{0}$ where δ is chosen to be smaller than $0.01\sigma_x^2$ and σ_x^2 is the variance of the input process [14]. For large sequences the choices of the initial conditions do not impact the performance of the RLS scheme.

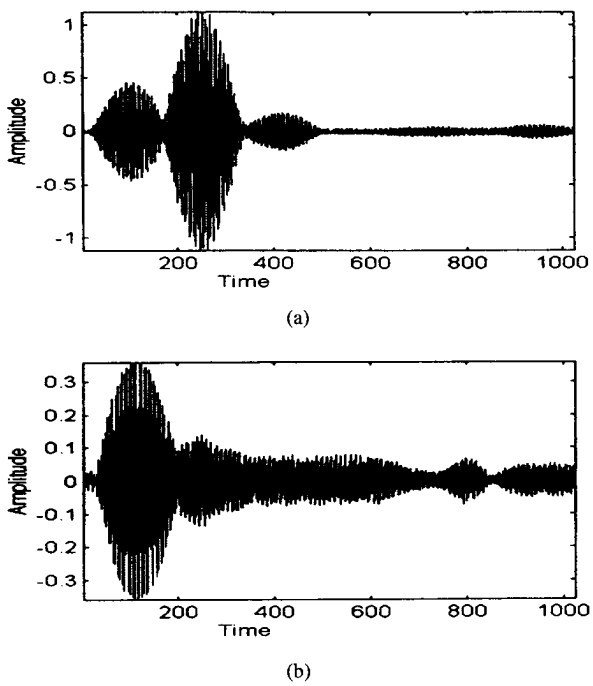

Fig. 3. (a) Backscattered: 108 KHz. (b) Backscattered: 150 KHz.

IV. Test Results

The first experiment examines backscatter data collected from a 2% spherical shell submerged in water. The mid-frequency enhancement for a 2% shell is known to center around a ka of 65 (refer to Fig. 1(a)). Experimental confirmation of the mid-frequency enhancement region for the fabricated shell was first conducted using a ping-by-ping sweep of narrow-band continuous wave pulses over incremental frequencies. The experimental data included the acoustic backscatter from the shell when excited by a pulse of length $T = 3.6$ with a cosine roll-off envelope for two different carrier frequencies with respective ka values of 63.2 and 87.8. The first signal is in the vicinity of the mid-frequency enhancement region. As shown in Fig. 3(a), the first echo in the backscattered return corresponds to the specular reflection while the subsequent echo is associated with the resonant part. In Fig. 3(b), which corresponds to the case of $ka = 87.8$, the subsequent echo is significantly attenuated as the pass-band of the excitation barely overlaps any part of the mid-frequency enhancement region. The desired and reference inputs to the adaptive estimator were the backscattered and incident signals. The adaptive system had only 16 tap weights in this experiment because of the short length of the incident burst and initial conditions were $\boldsymbol{P}(0) = 5000\,\boldsymbol{I}$ and $\boldsymbol{W}(0) = \boldsymbol{0}$. The plots of the error and output signals for these frequencies and their spectra are presented in Figs. 4(a)–(d) and 5(a)–(d), respectively. As expected, these plots show two narrow-band spectra corresponding to the specular and the

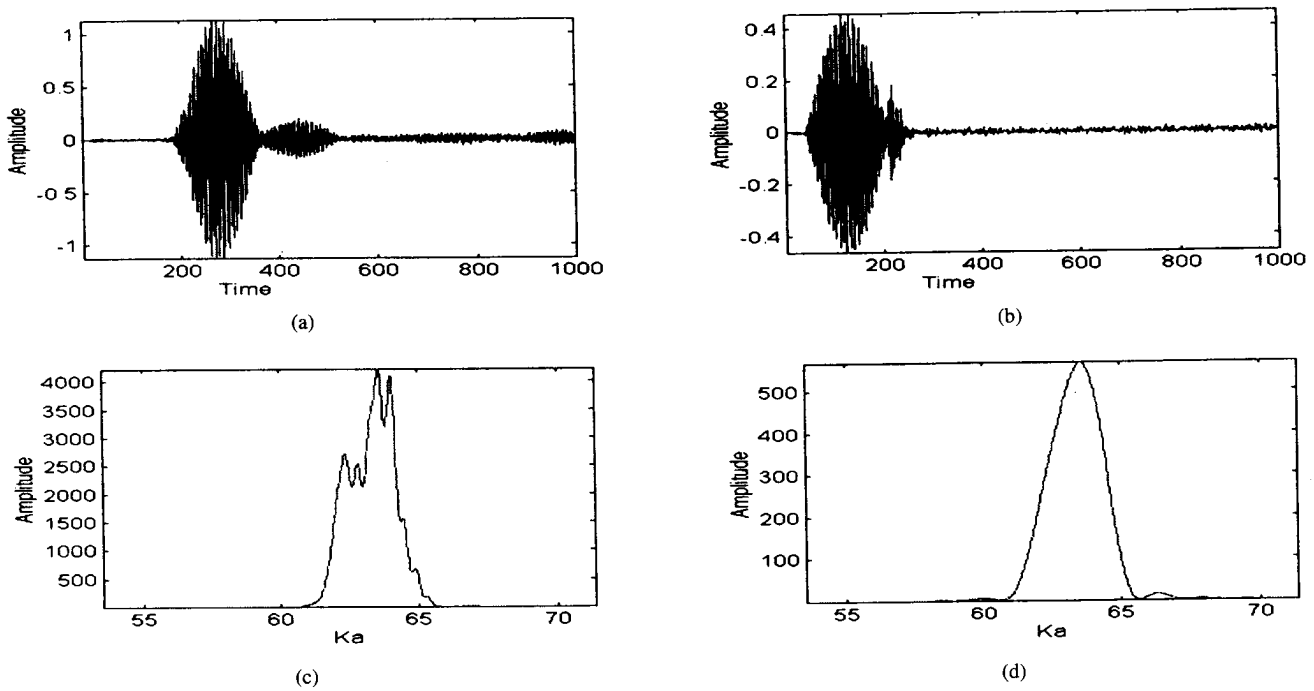

Fig. 4. (a) Error signal: 108 KHz. (b) Output of the adaptive system: 108 KHz. (c) Spectrum of the error: 108 KHz. (d) Spectrum of the output: 108 KHz.

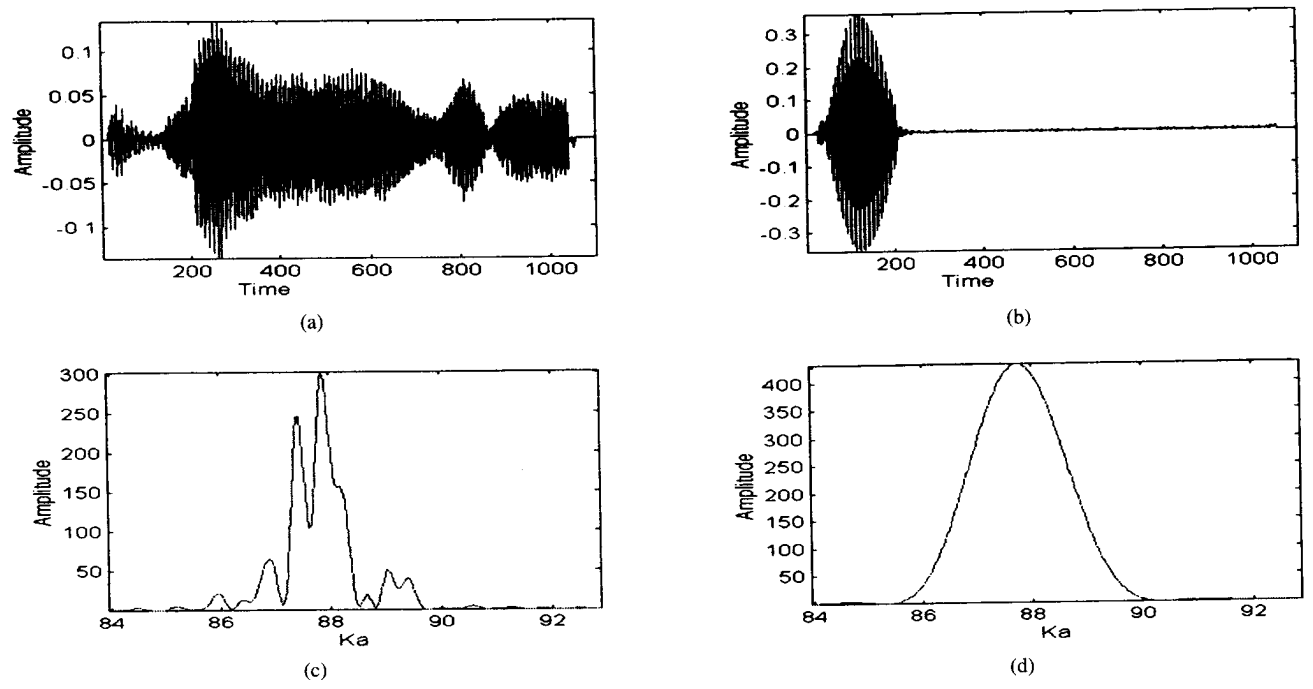

Fig. 5. (a) Error signal: 150 KHz. (b) Output of the adaptive system: 150 KHz. (c) Spectrum of the error: 150 KHz. (d) Spectrum of the output: 150 KHz.

resonant parts. The peak of the spectrum of the specular component is at the carrier frequency of the incident. For $ka = 63.2$ the spectrum of the error indicates a peak around $ka = 64.4$ which is in agreement with the theoretical results. In addition, the resonant component is substantially stronger in magnitude than the specular contribution as the frequency of excitation is close to that of the resonance. As the frequency of excitation increases the resonant component gradually disappears. This is due to the fact that the elastic shell responds as a linear system. The apparent shift in the spectra can be explained when the spectrum of the incident signal is compared with the frequency response of the resonant component. Owing to the fact that the incident is a tone burst with sinusoidal envelope, its spectrum has a large magnitude main lobe centered at the carrier frequency and some side lobes with smaller magnitudes. For $ka = 87.8$, the tail of the spectrum of the resonant component is overlapped with the main lobe, thus producing a small mid-frequency enhancement type behavior at the neighborhood of the carrier frequency. As expected the specular part has a spectrum with the same shape as the incident. The side lobes are not evident in these figures because of their low magnitudes relative to that of the main lobe. Note that the thickness quasi-

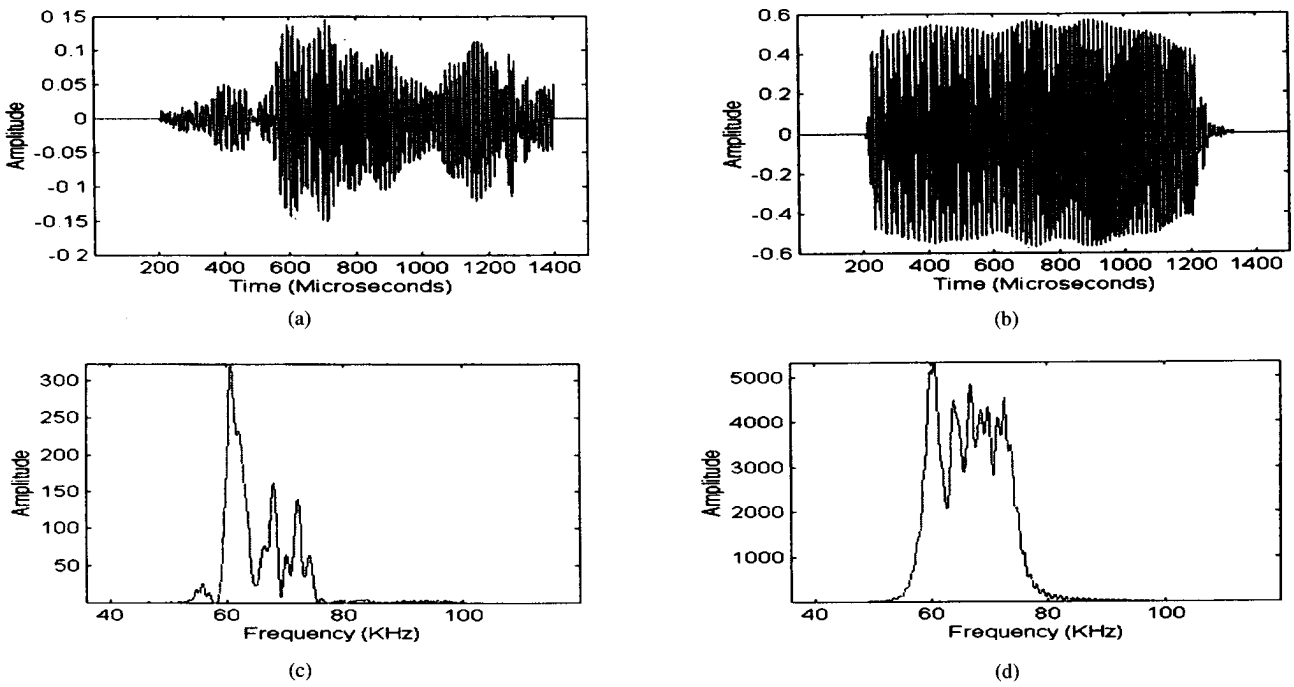

Fig. 6. (a) Error signal: 11.000. (b) Output of the adaptive system: 11.000. (c) Spectrum of the error: 11.000. (d) Spectrum of the output: 11.000.

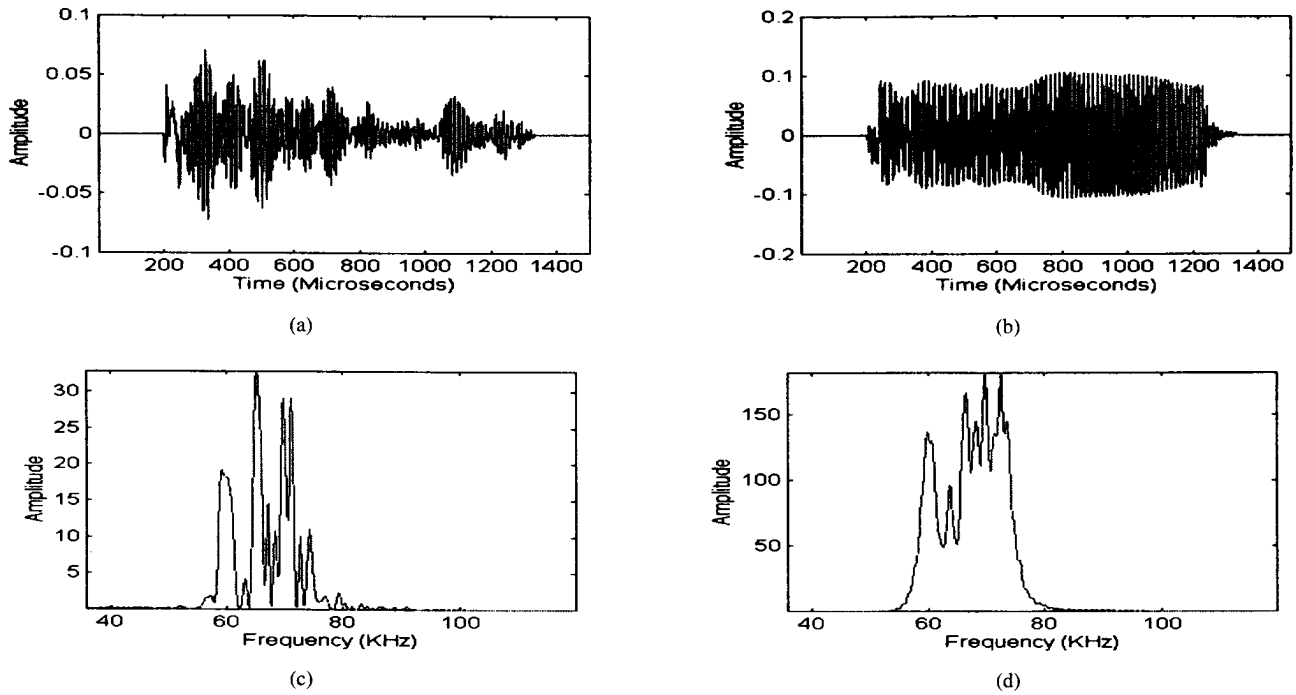

Fig. 7. (a) Error signal: 11.225. (b) Output of the adaptive system: 11.225. (c) Spectrum of the error: 11.225. (d) Spectrum of the output: 11.225.

resonance component is not seen in these signals as the frequency for this mode is well above the excitation frequency.

The adaptive estimation method was then applied to the data obtained from a submerged elastic target and an irregularly shaped concrete chunk of similar size. The elastic target had the form of a tapered, notched cylinder with flattened ends and rivets and an aspect ratio of 4 to 1. The incident signal was a wide-band linear FM with a time-bandwidth product of $TB = 20$. The signal was set to sweep over the mid-frequency band. The returns from each object were collected over 360° in 5° increments to produce 72 data records of differing aspect angle per object. Note that 0° corresponds to broadside incident. The measurements were performed under controlled operating and environmental conditions. The adaptive system had 32 tap weights and the initial conditions were $\boldsymbol{P}(0) = 5000\,\boldsymbol{I}$ and $\boldsymbol{W}(0) = \boldsymbol{0}$. The signal estimation was completed only after one pass over all the samples of the backscattered. Figs. 6(a)–(d), 7(a)–(d), 8(a)–(d), and 9(a)–(d) give the respective outputs of the adaptive system and the error signals together with their spectra for 0 and 225°, for the target and nontarget. As can be seen in these results, for the elastic target the output of the adaptive system, which

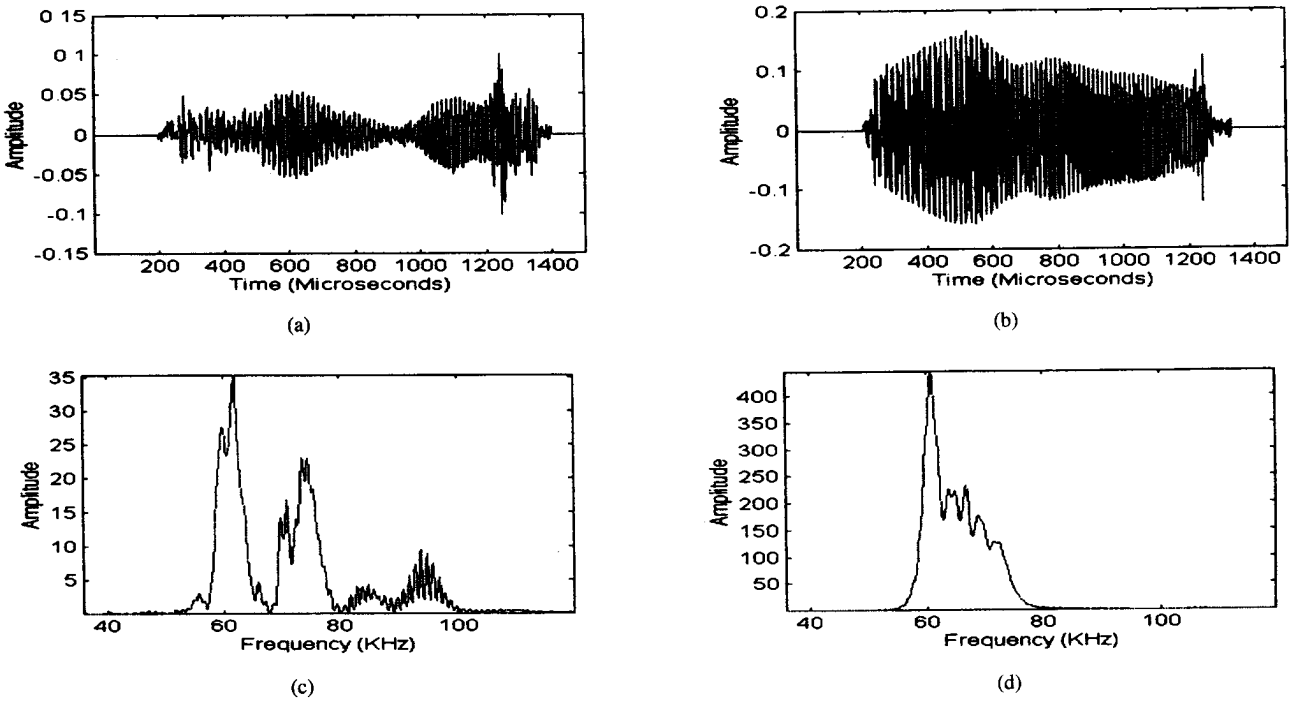

Fig. 8. (a) Error signal: 21.000. (b) Output of the adaptive system: 21.000. (c) Spectrum of the error: 21.000. (d) Spectrum of the output: 21.000.

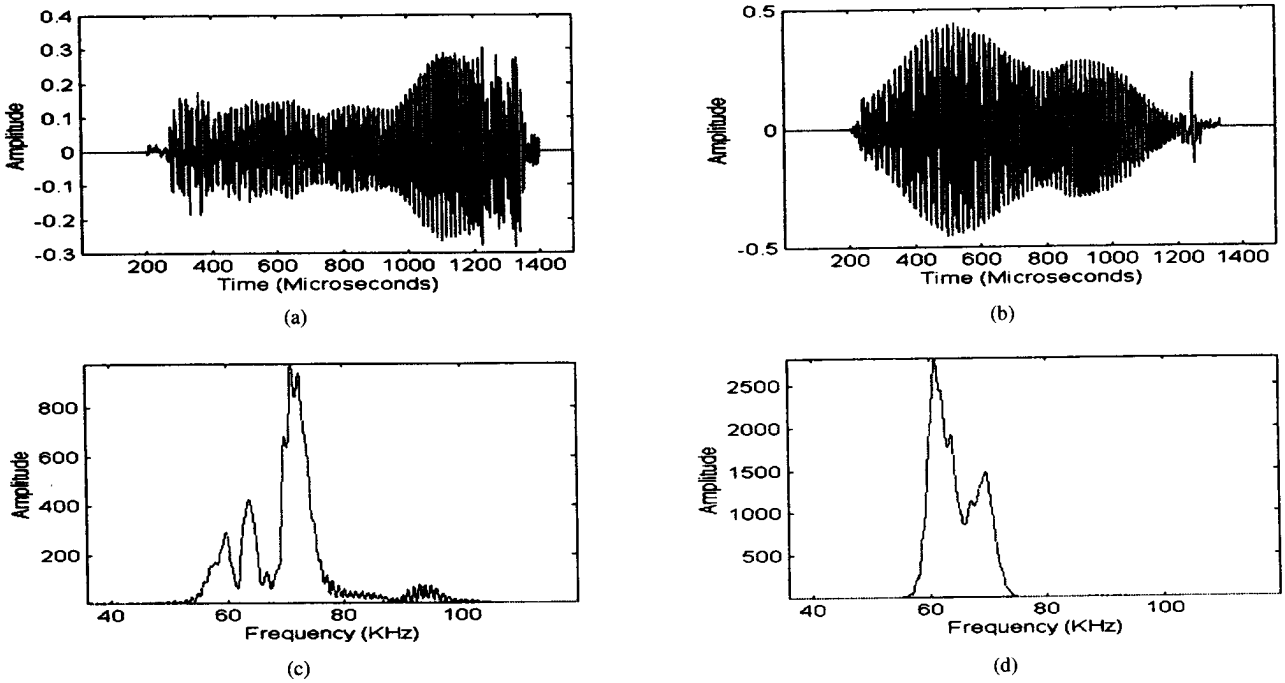

Fig. 9. (a) Error signal: 21.225. (b) Output of the adaptive system: 21.225. (c) Spectrum of the error: 21.225. (d) Spectrum of the output: 21.225.

provides the estimate of the specular part, has a broad-band spectrum while the error signal which provides an estimate of the resonant part generally contains one or more narrow-band components. For the nontarget anomaly, however, both the error and output signals were relatively wide-band. Based upon this criterion, over 89% of the cases were correctly identified. The remaining cases were not clearly distinguishable owing to the sensitivity of the adaptive system to strong subsequent specular returns whose onsets arise too quickly for the weights to converge. The results, however, verify the important conclusion that the adaptive estimation scheme is capable of identifying narrow-band phenomena present in the returns collected from targets and nontargets without requiring an underlying model for the returns.

Finally, to determine the effects of noise on the performance of the RLS parameter estimator and to demonstrate the robustness of the RLS learning, the above experiment, for zero aspect angle, was repeated for the elastic target when additive white Gaussian noise was injected to the backscattered signal. The variance of the

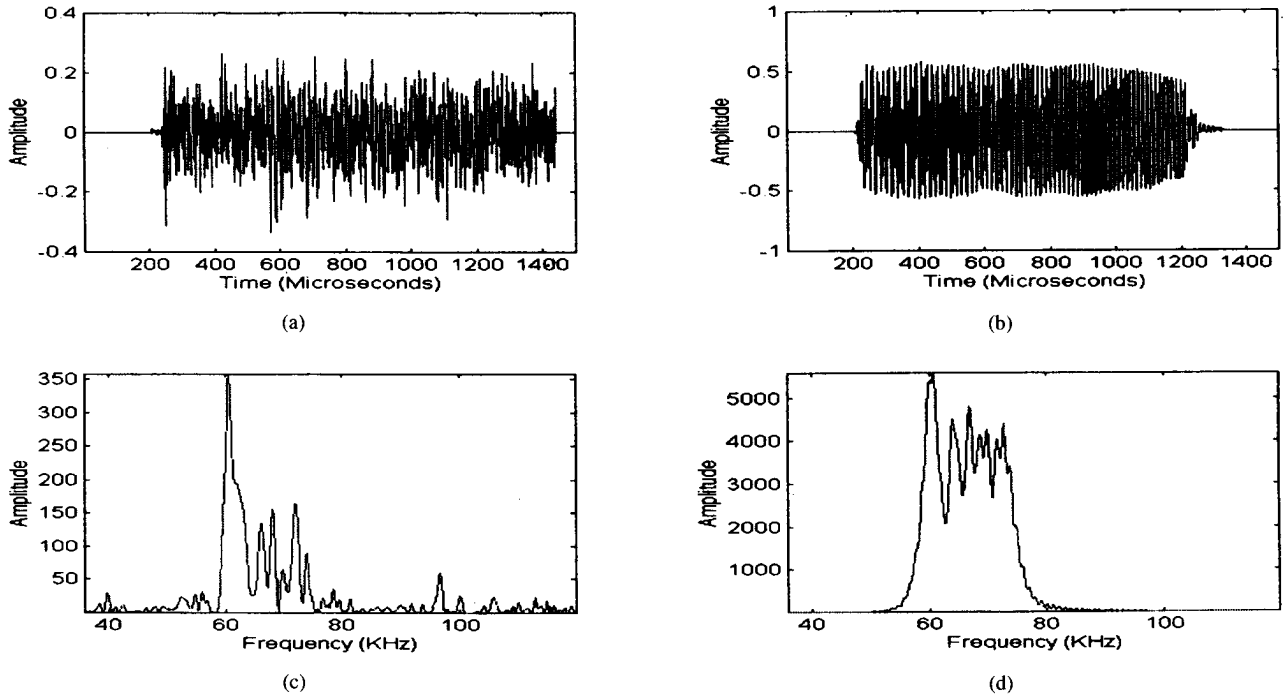

Fig. 10. (a) Error signal: 11.000. (b) Output of the adaptive system: 11.000. (c) Spectrum of the error: 11.000. (d) Spectrum of the output: 11.000.

additive noise was chosen so that the narrow-band SNR, i.e., the SNR computed within the bandlimits of the incident, was approximately 16 dB. Examination of the plots of the signals and their spectra in Fig. 10(a)–(d) which were obtained for one realization of the random noise, clearly reveals the robustness of the RLS learning scheme in the presence of noise.

V. Conclusions

The development of an adaptive system for detection and classification of underwater targets from acoustic backscatter was presented in this paper. The adaptive processing was shown to be an effective method for detecting the presence of submerged elastic targets. This is accomplished by determining the existence of a narrow-band resonance which is typically hidden in the acoustic backscatter. An adaptive estimator trained with the RLS rule was used, in this paper, to extract this resonant component in the acoustic backscatter from elastic targets. A unique aspect of this method for submerged targets is that no underlying model assumption is made about the elastic return. The adaptive system is trained to provide an estimate of the specular part which is highly correlated with the incident input. This enables the extraction of the resonant component at the error signal. The test results on experimental data obtained from 2% spherical shell, an elastic target and a nontarget (concrete chunk) were obtained which show the success of this scheme in isolating narrow-band phenomena which discriminates the target from nontargets. The extracted features can then be applied to a neural network classifier for final decision making.

Acknowledgment

The authors thank Bob Manning for his encouragement and support of this collaborative effort and Dr. Steve Kargl for his insightful review of the manuscript.

References

[1] L. Flax, G. C. Gaunaurd, and H. Uberall, "Theory of resonance scattering," *Phys. Acoust.*, vol. XV, pp. 191–292, 1981.

[2] L. G. Zhang, H. H. Sun, and P. L. Marston, "Mid-frequency enhancement of the backscattering of tone bursts by thin spherical shells," *J. Acoust. Soc. Am.*, vol. 91, pp. 1862–1874, Apr. 1992.

[3] G. S. Sammelmann, D. H. Trivett, and R. H. Hackman, "The acoustic of scattering by a submerged, spherical shell. I: The bifurcation of the dispersion curve for the spherical anti-symmetric lamb wave," *J. Acoust. Soc. Am.*, vol. 85, pp. 114–124, Jan. 1989.

[4] ——, "The acoustic of scattering by a submerged, spherical shell. II: The high-frequency region and thickness quasi resonance," *J. Acoust. Soc. Am.*, vol. 89, pp. 2096–2103, May 1991.

[5] R. H. Hackman and G. S. Sammelmann, "The acoustic of scattering by a submerged, spherical shell. III: Pole trajectories in the complex-ka plane," *J. Acoust. Soc. Am.*, vol. 90, pp. 2705–2717, Nov. 1991.

[6] S. G. Kargl and P. L. Marston, "Ray synthesis of the form function for backscattering from an elastic spherical shell: Leaky Lamb waves and longitudinal resonances," *J. Acoust. Soc. Am.*, vol. 89, pp. 2545–2558, June 1991.

[7] J. D. Murphy, J. George, A. Nagl, and H. Uberall, "Isolation of the resonant component in acoustic scattering from fluid-loaded elastic spherical shells," *J. Acoust. Soc. Am.*, vol. 65, pp. 368–373, Feb. 1979.

[8] J. Ripoche, G. Maze, and J. L. Izbicki, "A new acoustic spectroscopy: Resonance spectroscopy by the MIIR," *J. Nondestructive Evaluation*, vol. 5, no. 2, pp. 69–79, 1985.

[9] M. DeBilly, "Determination of the resonance spectrum of elastic bodies via the use of short pulses and Fourier transform theory," *J. Acoust. Soc. of Am.*, vol. 79, pp. 219–221, Feb. 1986.

[10] G. J. Dobeck, "Phase shift detection of the symmetric Lamb wave in acoustic returns," presented at Fourth Annu. Navy R&D Information Exchange Conf., Apr. 1993.

[11] J. P. Sessarego, J. Sageloli, P. Flandrin, and M. Zakharia, "Time-frequency analysis of signals related to scattering problems in acoustics-Part I: Wigner-Ville analysis of echoes scattered by a spherical shell, in *Wavelets*, J. M. Combes, A. Grossmann and P. Tchamitchian, Eds. New York: Springer-Verlag Series, 1987.

[12] J. Wilbur and S. G. Kargl, "Application of wavelets to acoustic resonance-elastic targets surrounded by biologics," in *Proc. IEEE Int. Conf. Acoust. Speech and Signal Process. (ICASSP'93)*, pp. IV.492–495, Minneapolis, MN, Apr. 1993.

[13] B. Telfer, H. Szu, and G. Dobeck, "Adaptive wavelet classification of acoustic backscatter," *SPIE (Wavelet Applications)*, vol. 2242, pp. 661–1668, 1994.

[14] S. Haykin, *Adaptive Filter Theory*, 2d Ed. Englewood Cliffs, NJ: Prentice-Hall, 1991.

[15] T. Soderstrom and P. Stoica, *System Identification.* Englewood Cliffs, NJ: Prentice-Hall, 1989.